[Short title + Author Name - P&H title] 17 (2024) 105938

Contents lists available at ScienceDirect

Arabian Journal of Chemistry

journal homepage: www.ksu.edu.sa

Biochar/poly(aniline-pyrrole) modified graphite electrode and electrochemical behavior for application in low-cost supercapacitor

Md. Mahabur Rahman [a,b], Abdulla Al Mamun [a], Hideto Minami [c], Md. Mahbubor Rahman [a], S. Manjura Hoque [d], Hasan Ahmad [a,*]

[a] Research Laboratory of Polymer Colloids and Nanomaterials, Department of Chemistry, Rajshahi University, Rajshahi 6205, Bangladesh
[b] Department of Chemistry, Pabna University of Science and Technology, 6600 Pabna, Bangladesh
[c] Graduate School of Engineering, Kobe University, Kobe 657-8501, Japan
[d] Materials Science Division, Bangladesh Atomic Energy Commission, Dhaka, Bangladesh

ARTICLE INFO

Keywords:
Biochar (BC)
Conducting copolymer
Oxidative polymerization
BC/P(Ani-Py) composite
Cyclic voltammetry
Galvanostatic charging-discharging

ABSTRACT

An attempt is made to use biochar (BC), a carbon rich low-cost green material, as a platform to house conducting polymer for fabricating stable graphite electrodes for application in next generation supercapacitor devices. Here, BC is first prepared from sucrose solution using a simple hydrothermal method. The seeded chemical oxidative copolymerization of aniline and pyrrole is then carried out at identical comonomer weight ratio using BC as seed particles. Two different BC to mixed monomer (w/w) ratios (1:0.7 and 1:1) have been used and the prepared composites are named as BC/P(Ani-Py)1:0.7 and BC/P(Ani-Py)1:1 respectively. Independent of composition, both BC seed and composite particles are spherical. The smooth homogeneous surface of BC turned heterogeneous after composite formation. The average size of BC seed particles is 2.56 μm and those of composites prepared at weight ratios of 1:0.7 and 1:1.0 are 2.72 and 2.90 μm respectively. Cyclic voltammetry (CV), galvanostatic charging discharging (GCD), and electrochemical impedance spectroscopy (EIS) are used to evaluate the electrochemical properties. Comparatively, the BC/P(Ani-Py)1:1 composite modified graphite electrode exhibited the highest capacitance value (274.27 F g^{-1} at a current density of 1.0 A/g) and is capable of acting as a supercapacitor electrode. A long-term cycling test of the BC/P(Ani-Py)1:1 modified electrode at a current density of 5.0 A/g displayed a capacitance retention of 96.6 % after 1000 cycles of charge and discharge, indicating a very good cycle stability.

1. Introduction

In the contemporary age, scientists around the world are paying tremendous attention to exploring zero-carbon emission-based renewable energy sources like solar, wind, geothermal, hydropower, ocean, biomass energy, etc. Of these energy sources, carbon compounds derived from biomass are attracting a lot of interest for usage as electrode materials in energy storage devices due to their economically viable nature, tunable physical/chemical properties, and environmental considerations (Mehmandoust et al., 2022; Xue et al., 2023). The versatility of the different types of biomass results in the emergence of unique structural and compositional characteristics in biochar (BC), a carbon dominant material. Additionally, the fine tuning of BC properties such as pore size distribution and surface functional groups during synthesis would allow optimization for specific application requirements. This tunability already enables tailored design of biochar-based materials for potential use in many areas, such as in soil remediation, catalyst/support, adsorbent, and energy storage (Nguyen et al., 2023; Lv et al., 2024; Visser et al., 2023; Lopes & Astruc, 2021; He et al., 2022; Lyu et al., 2020; Gao et al., 2018; Lin et al., 2023). From the energy storage perspective, BC has the potential to be used as a host for accommodating electroactive conducting polymers. In this regard, the favorable electrochemical property of BC as well as strong compatibility of BC with electroactive organic polymer should stimulate the performance of BC supported electroactive polymers (Park et al., 2021). The synergistic interaction between them would also provide stable environment friendly electrode material suitable for applications in supercapacitors and batteries (Aboughaly et al., 2023; Papadopoulou et al.,

* Corresponding author at: Research Laboratory of Polymer Colloids and Nanomaterials, Department of Chemistry, Rajshahi University, Rajshahi 6205, Bangladesh.
E-mail addresses: samarhass@yahoo.com, hahmad@ru.ac.bd (H. Ahmad).

https://doi.org/10.1016/j.arabjc.2024.105938
Received 25 March 2024; Accepted 24 July 2024
Available online 25 July 2024

2023; Wang et al., 2020a).

This is to mention that BC alone as electrode exhibits low energy storage capacity, low electrical conductivity, initial columbic losses, and swilling during electrochemical analyses which are all critical for electrochemical systems (Tan & Yu, 2024). On the other, conducting polymers are envisaged to narrow the gap between existing carbon-based energy storage materials and batteries to form units of intermediate specific energy because of their cost-effectiveness, non-toxicity, elegant electronic conductivity (10,000 S/cm), and high electronegativity (Kim et al., 2016). The presence of π-conjugated double bonds in conductive polymers promotes redox processes and has a significant charge storage capacity (Muthulakshmi et al., 2006; Moyseowicz et al., 2023; Rashid et al., 2020; Ali et al., 2022). Furthermore, the conductivity of conductive polymer such as polyaniline (PAni), polypyrrole (PPy) and polythiophene (PTh) virtually depends on the arrangement of polymer chains and extent of conjugation. It is observed that copolymerization reaction of these monomers enhances the structural regularity of main chains, the conjugation and hence the ultimate conductivity (Kim et al., 2019; Wang et al., 2019; Lu et al., 2021; Dhibar et al., 2015). These copolymers are also expected to demonstrate reduced volume expansion due to internal stress during the charging-discharging process and thus maintaining electrochemical performance (Ma et al., 2023). In this context, chemical oxidative copolymerization of aniline and pyrrole on a BC support would be interesting from the view point of measuring its potentiality as electrode materials in supercapacitor application. The preparation of poly(aniline-pyrrole) or P(Ani-Py) copolymer would also add extra advantages due to the combination of individual properties of both PAni and PPy in a single material (Zhou et al., 2008; Wang et al., 2020b). This is to mention that based on energy storage mechanism two major types of supercapacitor/energy storage devices viz., electric double layer capacitor (EDLC) and pseudocapacitor are available (Zhang et al., 2023; Zhang et al., 2024b). EDLCs store energy through the physical separation of charge at the interface between the electrode and the electrolyte, while, pseudocapacitors store energy through fast and reversible surface redox reactions at the electrode–electrolyte interface. Conducting P(Ani-Py) copolymer alone can be classified as a pseudocapacitor material and carbon rich BC as a EDLC material. A combination of both EDLC and pseudocapacitor i.e., BC and P(Ani-Py) copolymer in a single composite would therefore combine the advantages of both, utilizing both the double-layer effect and reversible redox reactions (Yan et al. 2020; Zhang et al., 2023a). In addition to the supercapacitor/energy storage devices, such composites can find applications in inkjet electronic printing, antioxidant, sensor, adsorbent, microwave absorption, catalysts and anticorrosive formulation (Rahman et al., 2023; Ahmad et al., 2016; Debnath et al., 2019; Hajiabdolah et al., 2020; Saharan et al., 2023; Sankar & Ramesan, 2022; Thi et al., 2020; Khan et al., 2022; Govindaraju & Prakash, 2015; Idrees et al., 2018; Sun et al., 2022; Chaudhary & Kaur, 2015).

A few research works related to hosting conductive P(Ani-Py) copolymer on different types of supports have been available in literature. For example, Dhibar *et al.* prepared $CuCl_2$ doped P(Ani-co-Py)/multi walled carbon nanotubes [poly(Ani-*co*-Py) Cu CNT] by in-situ chemical oxidative polymerization and observed the highest capacitance value of 274.27 F g^{-1} at a scan rate of 0.5 A g^{-1} (Dhibar et al., 2015). Lu *et al.* prepared poly(Ani-co-Py)/single walled carbon nanotubes (SWCNTs) via electropolymerization technique and observed improvement in thermoelectric properties and conductivity (Lu et al., 2021). Moyseowicz *et al.* devised poly(aniline-co-pyrrole)/thermally reduced graphene oxide (TRGO) by carrying out oxidative polymerization and observed the highest specific capacitance (274.27 F g^{-1} at 0.2 A g^{-1}) at the TRGO content of 20 wt% (Moyseowicz et al., 2018). Dong *et al.* demonstrated that inclusion of inorganic Ni-MnO_2 at a mass ratio of 1/5 to aniline and pyrrole mixed monomer increases the specific capacitance and cycle stability (Dong et al., 2020). In a different approach, in-situ chemical polymerization of pyrrole was first carried out in presence of PAni nanofibers to obtain core–shell type poly(Ani-co-Py) and finally the suspension was mixed with reduced GO (Liu et al., 2021). The prepared composite with a mass ratio of GO to core–shell poly(Ani-co-Py) of 9/1 exhibited the maximum specific capacitance. Recently, Oliveira *et al.* reported the supercapacitive performance of PPy/PAni modified carbon-graphite (CG) electrode, prepared by subsequent electropolymerization (Oliveira et al., 2024). The CG/PPy/PAni electrode had specific capacitance of 3416 mF cm^{-2} at a current density of 2 mA cm^{-2} and the retention capacity was 76 % after 850 galvanostatic charge–discharge (GCD) cycles. It is evident from the above literature review that only some limited researches are available on GO or CNT supported P(Ani-Py) copolymers. Despite some advantages of GO or carbon nanotube (CNT), environmental risk in synthesis and the high cost increases the risk of their applications (Kim et al., 2024). Moreover, their syntheses require complex procedure with costly starting materials. From this perspective, biomass can be a sustainable and ideal carbon source for the large-scale production of BC due to its low cost, renewability, and CO_2 neutrality.

Herein, for the first time, attempt is made to realize high performance conductive aniline-pyrrole copolymer functionalized BC modified graphite electrode for application in supercapacitors. In this experiment, BC was produced by hydrothermal carbonization of sucrose, which is easily accessible, comparatively safer and greener. The P(Ani-Py) functionalized BC composite was then produced by in-situ chemical oxidative copolymerization of aniline and pyrrole in presence of BC seed, utilizing an oxidant. Two different weight ratios of BC to mixed monomer (1:0.7 and 1:1.0) were employed and the obtained composites were named as BC/P(Ani-Py)1:0.7 and BC/P(Ani-Py)1:1 respectively. The preparation of composites is detailed in Fig. S1. The resultant composites were examined using scanning electron microscope (SEM), transmission electron microscope (TEM), X-ray photoelectron spectroscopy (XPS), Fourier transform IR (FTIR) and thermogravimetric analyzer. The overall characterizations confirmed the formation of poly(aniline-pyrrole) copolymer domains on the surface of BC seed particles. The electrochemical properties of the as synthesized BC, P(Ani-Py), BC/P(Ani-Py)1:0.7, and BC/P(Ani-Py)1:1 were evaluated by cyclic voltammetry (CV), galvanostatic charge–discharge (GCD), and electrochemical impedance spectroscopy (EIS). The BC/P(Ani-Py)1:1 composite modified graphite electrode exhibited the best capacitive performance. This work gives readers an insight on the utility of low-cost biomass derived BC as emerging support materials for conducting P(Ani-Py) copolymer for potential applications in supercapacitor/energy storage devices as well as in catalysis, adsorbents, inkjet materials etc.

2. Materials and methods

2.1. Materials

Monomer grade aniline and pyrrole, as well as reagent grade sucrose, were acquired from Sigma-Aldrich Chemie GmbH, USA and utilized directly without purification. Ammonium persulfate, $(NH_4)_2S_2O_8$, and HCl from Merck, India were used as oxidant and dopant respectively. Triton X-405 solution from Sigma-Aldrich Chemie GmbH, USA was used to stabilize the suspension. KCl electrolyte from Merck, India, binder polyvinylidene fluoride (PVDF) and N-methyl-2-pyrrolidone (NMP) both from Sigma-Aldrich Chemie GmbH, USA were employed to make the working electrode for CV measurements. Reverse osmosis and UV radiation were used to extract Distilled deionized (DD) water from Puricom, Taiwan.

2.2. Preparation of BC

BC seed powders were prepared using the hydrothermal method (Sevilla & Fuertes, 2009). A 0.8 M sucrose solution was made by dissolving sucrose in 100 mL of DD water. The solution was then placed in a Teflon-lined stainless-steel autoclave and subjected to heating in a hot air oven at 180 °C for 135 min. The resulting black precipitate was

separated by centrifugation at 6000 rpm and subsequently washed with DD water until the supernatant turned clear.

2.3. Preparation of BC/P(Ani-Py)

Electroactive BC/P(Ani-Py) composites were prepared through in-situ seeded chemical oxidative copolymerization involving aniline and pyrrole in the presence of BC seed particles. Two different weight ratios of BC to mixed monomer (e.g., 1:0.7 and 1:1.0) were applied for such preparations. A homogeneous dispersion from BC seed particles, requisite amount of monomers and Triton X-405 was first prepared in 50 mL of 0.1 M HCl by magnetic stirring. Then, after temperature equilibration at 25 °C, APS aqueous solution was gradually added under constant stirring at 500 rpm. The pH of the reaction mixture was maintained near 1.0 and the copolymerization reaction was continued in an inert N_2 atmosphere for 24 h. Finally, the black suspension was obtained, washed repeatedly with DD water until the supernatant became clear. Table S1 shows the amount of reactants used and reaction conditions.

2.4. Material characterizations

The surface morphology and size distribution of prepared particles were analyzed by SEM (JSM-6510, JEOL, Tokyo, Japan) operated at 20 kV and TEM (JEM-1230, JEOL, Japan). XRD (Bruker D8 Advance, Germany) was used to assess crystallinity index of synthesized materials. FTIR (Perkin Elmer, FTIR-100, USA) was used to check the variation in phase and structural functionality following seeded chemical oxidative copolymerization. The surface elemental composition was evaluated by XPS (PHI X-tool, ULVAC-PHI, Inc., Japan). The XPS was equipped with a monochromatic Al Kα radiation (1486.6 eV) at 15 kV, 50 W and an X-ray current of 20 mA. The acquisition area and take-off angle were kept fixed at 20 μm and 45° respectively and the pressure in the measurement chamber was 8.0×10^{-7} pa. The step size was 1.0 eV for the both the survey spectra and high resolution spectra (pass energy 280 eV). The thermal properties for the dried samples were checked by Thermogravimetric analyzer, TGA (STA 8000, Perkin Elmer, Netherlands). The sample was heated under a flowing nitrogen atmosphere at a heating rate of 20 °C min^{-1} and the mass loss in percent was recorded. The initial mass of dried sample was maintained at around 10 mg.

2.5. Electrochemical measurements

The CV, GCD, and EIS analyses were worked out using Corrtest Electrochemical Workstation, CS350, China, in a three-electrode system using 1.0 M KCl as the electrolyte. Graphite rod, platinum wire, and Ag/AgCl were used as the working, counter, and reference electrodes, respectively. For fabricating the working electrode, the active part of graphite rod was coated with homogeneous slurry made from a mixture of electroactive material and PVdF binder mixed at a 90:10 (w/w) ratio in the N-methyl pyrrolidone (NMP) solvent. The modified graphite electrode was then dried for 12 h at 60 °C in an electric oven. The mass loading of the electroactive substance on the electrode was maintained between 1.2 to 2.0 mg on a surface area of 6.15 cm^2.

Prior to the CV experiment, N_2 gas was bubbled for 10 min. The working electrode was submerged in the electrolyte solution. The CV measurements were done in the potential range of −0.2 V to + 0.6 V at an optimized scan rate of 50 mV s^{-1} at 25 °C for BC, P(Ani-Py), BC/P (Ani-Py)1:0.7 and BC/P(Ani-Py)1:1 modified graphite electrodes, respectively.

GCD experiments were executed with the identical modified electrodes in the same electrolyte solution at a fixed current density of 1.0 A g^{-1}. The same measurement was performed at variable current densities for the BC/P(Ani-Py)1:1 composite modified graphite electrode. EIS measurement was conducted in the frequency range of 10^{-2} to 10^5 Hz to investigate the electrochemical behavior of the prepared electroactive composite materials. The experimental EIS data were processed using the ZSimpWin software. The specific capacitance (C_s) of the respective material was calculated from GCD curve using Eq. (1).

$$C_s = \frac{I \times \Delta t}{m \times \Delta V} \tag{1}$$

where, ΔV is the discharge potential excluding the IR drop, m is the mass (g) of electroactive materials, I is the discharge current (A) and Δt is the discharge time(s). The energy density, E (W h Kg^{-1}) and power density, P (W kg^{-1}) for composite modified graphite electrode were also estimated from GCD curve using the Eqs. (2) and (3) respectively:

$$E = \frac{C_s \times (\Delta V)^2}{2 \times 3.6} \tag{2}$$

$$P = \frac{E \times 3600}{\Delta t} \tag{3}$$

3. Results and discussion

3.1. Characterizations

FTIR spectra for BC seed, reference P(Ani-Py), BC/P(Ani-Py)1:0.7 and BC/P(Ani-Py)1:1 are recorded for determining the surface functionality and their formation. Fig. S2a displaying the spectrum of BC seed, shows the bands at 1692, 1639 and 1559 cm^{-1} for C=O (carbonyl, quinone, ester or carboxyl) and aromatic C=C vibrations, respectively (Labbé et al., 2006; Sun et al., 2018). In contrast, the bands in the 1000–1450 cm^{-1} range are assignable to C=C stretching, C–O (ester or ether) stretching and phenolic O=H bending vibrations, respectively (Zhou et al., 2008; Li et al., 2020). While, the bands at about 2930 and 3000–3700 cm^{-1} are attributable to stretching vibrations of aliphatic C=H and absorbed moisture derived O=H. The bands in the region of 875–750 cm^{-1} represent aromatic C–H out-of-plane bending vibrations (Li et al., 2020). Spectrum of reference P(Ani-Py) copolymer (Fig. S2b) shows broad band at 1559 cm^{-1} with a shoulder signal at 1639 cm^{-1} represent quinonoid phenyl ring C-C stretch of PAni segment and C=C/C-C stretch of PPy segment (Zhou et al., 2008; Wang et al., 2020b). This is an indication of the bond formation between aniline and pyrrole. Additionally, the band at 1112 cm^{-1} possibly belongs to the C–H in-plane bending vibration of the substituted benzene of PAni (Zhou et al., 2008). While, the bands at around 1390 and 1480 cm^{-1} are due to semiquinonoid ring (=N-ring) and C=C stretching vibration of benzenoid ring of PAni (Dong et al., 2020; Hammad et al., 2018; Lv et al., 2023). The intense absorption signal appears at 960 cm^{-1} is assignable to C=C out-of-ring deformation for PPy segment (Antony & Jayakannan, 2011). The higher reactivity of pyrrole (2.16) compared to aniline (0.13) is expected to produce copolymer with blocky character rich in pyrrole unit (Antony & Jayakannan, 2011). So, from the FTIR analysis it is reasonable to say that chemical oxidative polymerization produced random copolymer of P(Ani-Py) with rich pyrrole content. Comparatively, in the spectra of BC/P(Ani-Py)1:0.7 (Fig. S2c) and BC/P(Ani-Py) 1:1 (Fig. S2d) composites, the signals due to BC, particularly in the range of 1000–1450 cm^{-1}, are dominated when BC to monomer weight ratio is 1:0.7. But at the higher weight ratio of 1:1.0 the signal intensity due to P (Ani-Py) increased appreciably. The above findings confirm the formation of BC modified conducting composites.

The size and surface morphology observed by SEM images are shown in Fig. 1. It is evident that BC seed particles (Fig. 1a) are almost spherical and bit polydispersed. The surface is visibly smooth and homogeneous. The average diameter and coefficient of variation (CV) of BC seed particles measured by ImageJ software are 2.56 μm and 11.66 % respectively. Comparatively, the P(Ani-Py) copolymer particles shown in Fig. 1b are aggregated though the suspension was apparently stable. Particles are probably organized into clusters during the drying of the samples. The average size and CV of P(Ani-Py) particles are 0.22 μm and 33.36 %, respectively. In contrast to the smooth homogeneous surface of

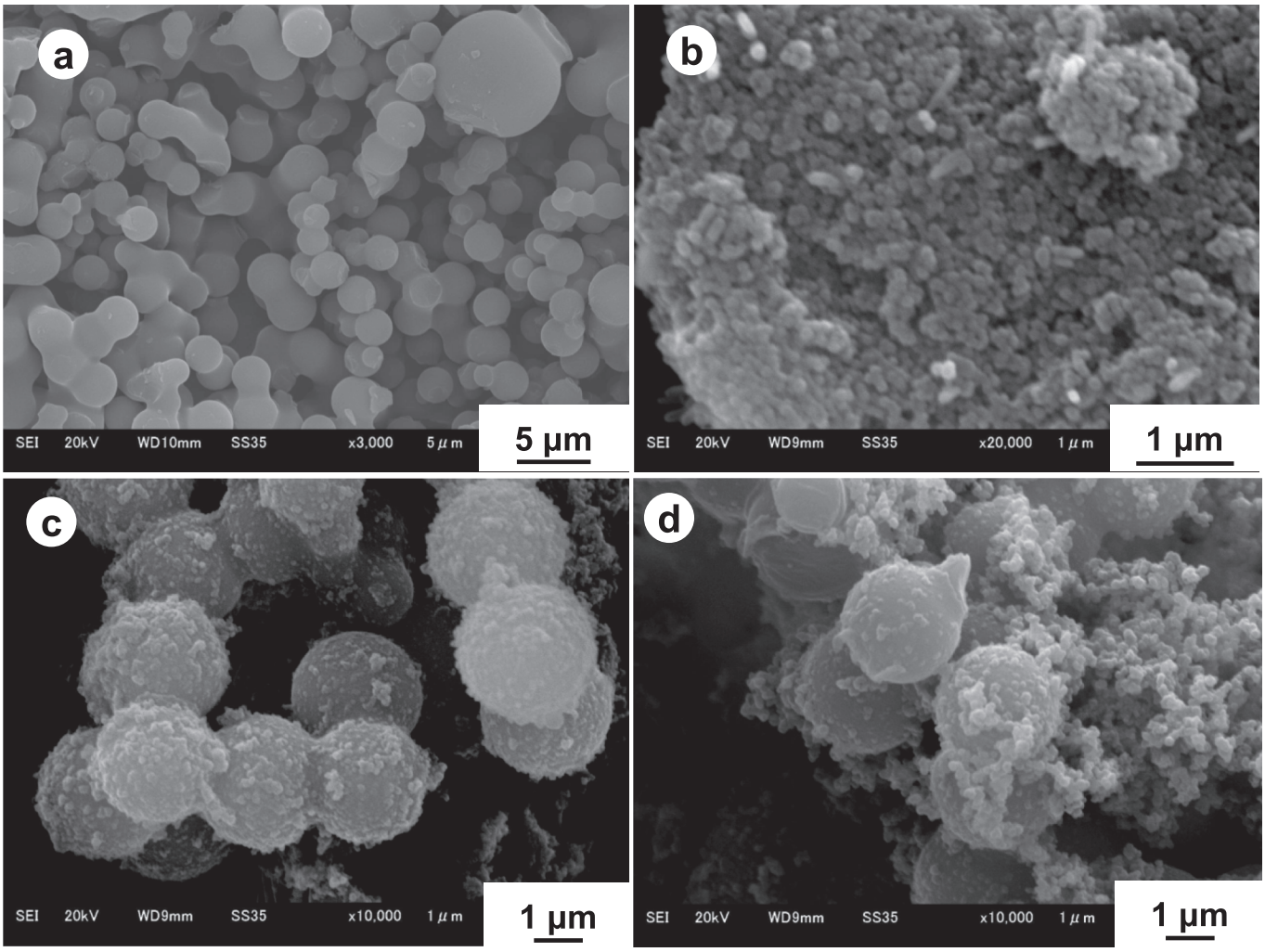

Fig. 1. SEM images of (a) BC seed particles, (b) P(Ani-Py) particles, (c) BC/P(Ani-Py)1:0.7 and (d) BC/P(Ani-Py)1:1 composite particles.

BC seed particles, the surfaces of BC/P(Ani-Py) composites turned heterogeneous after seeded chemical oxidative copolymerization. It can also be ascertained that smaller P(Ani-Py) copolymer particles are firmly adhered to the surface of BC microspheres. At a lower weight ratio of 1:0.7 of BC to monomer (Fig. 1c) independent smaller particle is hardly observed. But, at a higher weight ratio of 1:1.0 (Fig. 1d) some free smaller particles, presumably P(Ani-Py) copolymer particles, might have formed. It is also probable that increased production of smaller copolymer particles at higher monomer content produced hairy network around the BC seed microspheres. Whatever the findings, optimization of the BC to monomer weight ratio is important for preventing the secondary nucleation and hence, the formation of free copolymer particle. The average diameters and CVs of BC/P(Ani-Py)1:07 and BC/P (Ani-Py)1:1 composites are 2.72 μm, 6.5 % and 2.90 μm, 9.6 %, respectively. Hence, it is apparent from the average size distribution that average size of BC increased following seeded oxidative copolymerization. A comparison among SEM images suggests that BC surface contained numerous active sites to fix large number of P(Ani-Py) copolymer particles and thus enhanced the ultimate stability of copolymer particles as well as of composite particles. The mode of interaction between BC and electroactive P(Ani-Py) copolymer layer during seeded copolymerization is possibly initiated by the formation of hydrogen bond among –OH/ester/ether/carboxyl functionalities on BC seed and –NH functionality in the copolymer chain. The successful preparation of composite structure comprising conductive P(Ani-Py) and BC may thus be an effective way to obtain relatively high-performance supercapacitor electrode material.

Fig. S3 demonstrates TEM images of BC seed particles, P(Ani-Py) particles, BC/P(Ani-Py)1:0.7 and BC/P(Ani-Py)1:1 composite particles. The dark color of BC (Fig. S3a) indicates that BC seed particles are solid spheres as electronic light of TEM passed through dense areas usually produced darker pixels. Compared to SEM image (Fig. 1b), P(An-Py) copolymer particles appears (Fig. S3b) fairly stable and spherical. The surfaces of composite particles (Fig. S3c,d) are hairy and rough. Some sort of aggregation occurred during drying of the composite suspension. The orientation of smaller particles in a hairy network apparently occurred at higher BC to monomer weight ratio, as anticipated for BC/P (Ani-Py)1:1 composite from SEM image (Fig. 1d). The average diameters measured for BC seed, P(Ani-Py), BC/P(Ani-Py)1:0.7 and BC/P(Ani-Py) 1:1 are 2.73, 0.13, 3.84 and 7.28 μm respectively. The higher polydispersity index possibly affected the actual measurement.

From XPS measurement, the distributions of carbon and nitrogen species were analyzed via deconvolution of C1s and N1s core line spectra as illustrated in Fig. 2. The survey spectra (not shown) indicate that nitrogen content in P(Ani-Py) particles is 4.47 at.% and this reduces to 0.98 and 2.20 at.% in BC/P(Ani-Py)1:0.7 and BC/P(Ani-Py)1:1 composites respectively. The deconvolution of C1s core line spectrum of P(Ani-Py) particles (Fig. 2a) resulted in three components attributable to C=C (~284.5 eV), C=N (~285.8 eV) and carbonyl/quinone groups (~287.9 eV) and a satellite peak due to C-N group (~290.9 eV) (Moyseowicz et al., 2018). An additional peak at 282.2 eV possibly came from metal carbide, correspond to indium plate used for mounting sample

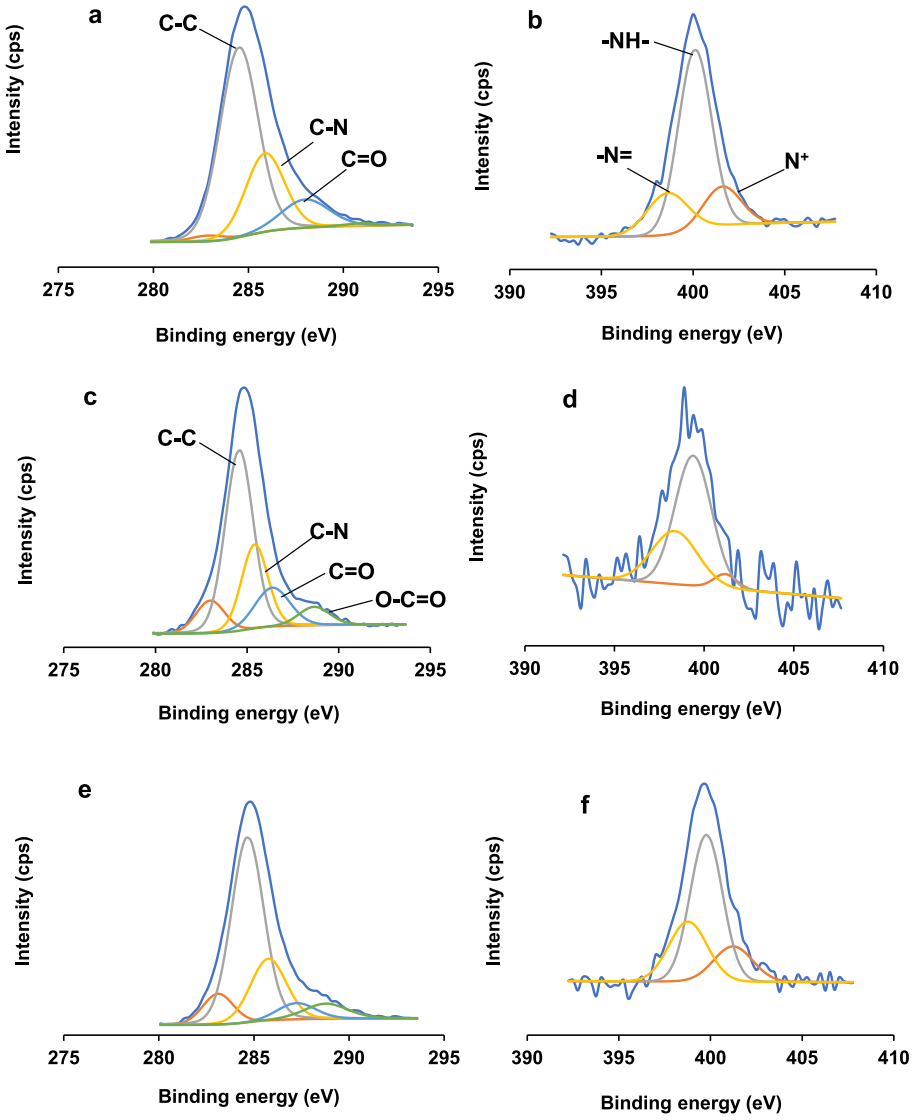

Fig. 2. XPS deconvoluted (a,c,e) C1s and (b,d,f) N1s core line spectra of (a,b) P(Ani-Py) particles, (c,d) BC/P(Ani-Py)1:0.7 and (e,f) BC/P(Ani-Py)1:1 composite particles.

(Hou et al., 2022). Comparatively, the C1s core line spectra of composites (Fig. 2c,e) can be distinguished into four clear components corresponding to C=C (~284.6 eV), C-N (~285.7 eV), carbonyl/quinone (~287.24 eV) and carboxyl (~288.78 eV) groups (Moyseowicz et al., 2018). The introduction of BC in composites significantly reduces C-N content from 25.6 % in P(Ani-Py) to 16.3 and 21.1 % in BC/P(Ani-Py) 1:0.7 and BC/P(Ani-Py)1:1 composites respectively. The addition of BC increases the metal carbide content from 1.7 % in P(Ani-Py) to around 9.1 % in composite particles. The presence of high carboxyl content (1–6 %) in composites also reaffirms carboxyl functionality of BC in composites.

On the other, the deconvoluted N1s core line spectra of P(Ani-Py) particles and composites show three peaks at around 398.6, 400.1 and 401.2 eV, assignable to imine (=N=), amine (=NH=) and oxidized amine (N^+) groups. The most dominant nitrogen component in P(Ani-Py) particles (Fig. 2b) is amine group (65.2 %) followed by imine group (18.8 %), implying predominance of PANi in the protoemaraldine form (Golczak et al., 2008). But, in the BC/P(Ani-Py)1:1 composite (Fig. 2f) the variation between amine (48.8 %) and imine (36.7 %) content is narrowed. Comparatively, the variation between amine (63.2 %) and imine (32.3 %) content in the BC/P(Ani-Py)1:0.7 composite (Fig. 2d) is slightly widened but still lower than that in the reference P (Ani-Py) particles. It looks probable that oxidizing nature of BC due to protonation of carbonyl and carboxyl groups preserved higher amount of oxidized imine group along the copolymer chain in composites (Lim et al., 2001). Significantly higher amount of amine and imine groups in composites despite lower contribution from BC indicates that large contact area and strong hydrogen bonding interaction favored the formation of composite structure.

The crystalline phase of the respective BC microparticles, reference copolymer particles and composites particles were evaluated by XRD patterns as shown in Fig. S4. The diffraction pattern of BC (Fig. S4a) suggests that BC seed derived from sugar solution is pure without any crystalline materials. The broad peak in the two-theta region of 18-30° generally represent amorphous carbon, preferably composed of aromatic compounds oriented in random fashion (Hara et al., 2004; Gale et al., 2021). The crystallinity index of BC particles, calculated by the Segal equation, is 17 %, while for reference copolymer particles it is 27 %. Comparatively, the values of crystallinity index for composites prepared with BC to monomer (w/w) ratios of 1:0.7 and 1:1.0 are 22 % and 24 %, respectively. Obviously, the seeded chemical oxidative polymerization and subsequent coverage of BC surface by amorphous P(Ani-Py) copolymer slightly increases the crystallinity than BC seed particles.

A TG analysis was conducted to understand the stability of BC/P(Ani-

Py) composite particles. It is evident that all materials (Fig. 3), independent of nature, show an initial mass loss up to 101 °C. This initial mass loss is associated with driving off of smaller molecules like absorbed CO_2 and water vapor. The second mass loss region for reference P(Ani-Py) particles is minimum (~258 °C), while that of neat BC seed is maximum (~261 °C). The addition of BC and formation of composite structure slightly improved the thermal stability of BC/P(Ani-Py) composites and decomposition temperature lies between those of BC (~258 °C) and reference P(Ani-Py) (~261 °C) particles. Comparatively, reference P(Ani-Py) particles show a distinct third mass loss region at around 468 °C. The two mass loss regions (at ~ 261 and ~ 468 °C) for reference P(Ani-Py) are ascribed to the decomposition of low and high molecular weight copolymers formed during copolymerization reaction. However, such behavior is not distinctly visible in composite particles. The residual mass is varied between 3 to 10 % with BC/P(Ani-Py)1:0.7 (curve c) has the minimum residual mass (3 %) and BC/P(Ani-Py)1:1 (curve d) has the maximum residual mass (10 %). This behavior is not expected as total mass is organic in nature. Even, carbon rich BC showed 5 % residual mass. There is report that as the temperature of BC is increased from 700 to 1000 °C, solid carbons are repolymerized, aromatized and pores are generated (Yasim-Anuar et al., 2022). This transition might have increased the stability to thermal degradation and produced residual mass in BC. The highest residual mass in BC/P(Ani-Py)1:1 composite particles might suggest that higher copolymer content improved the thermal stability towards such transformation as happened in case of native BC (curve a). It is also probable that difference between volume and mass ratios of BC and composite particles contributed to the variation in residual mass. The residual mass of around 6 % observed for P(Ani-Py) possibly came from burnt carbon residue. Overall, the deviation of TG thermograms of composites from those of BC and pure copolymer indicates that BC is modified with electroactive copolymer domains.

3.2. Electrochemical performance

Three electrode systems were used to conduct electrochemical performance in a 1.0 M KCl electrolyte solution. The working graphite electrode was modified with our prepared materials. The CV curves were obtained in the potential window of −0.2 V to + 0.6 V, at an optimal scan rate of 50 mV s^{-1}. The above potential window was selected as the best characteristic CV peak appeared in that region. The CV curves of rectangle shape demonstrated the good capacitive performance of the P (Ani-Py) and BC/P(Ani-Py)1:1 composite modified graphite electrodes

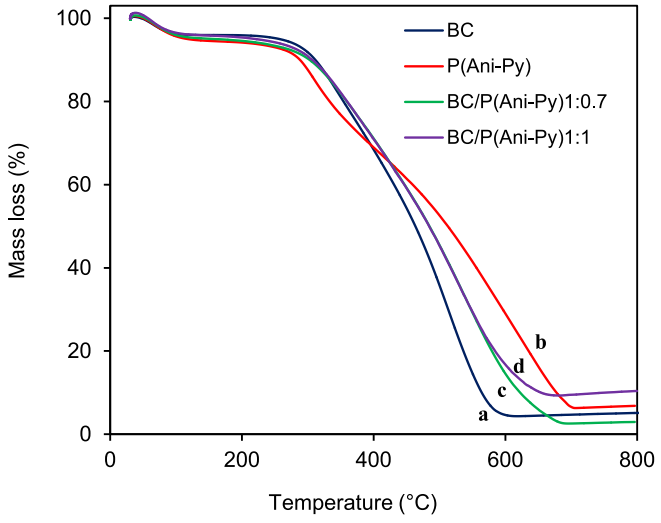

Fig. 3. TG thermograms of (a) BC seed particles, (b) P(Ani-Py) particles, (c) BC/P(Ani-Py)1:0.7 and (d) BC/P(Ani-Py)1:1 composite particles.

(Fig. 4a). The doping/de-doping reaction caused the faradaic redox process to occur reversibly. The current responses improved in the order of P(Ani-Py) > BC/P(Ani-Py)1:1 > BC/P(Ani-Py)1:0.7 > BC. It can be seen that with the increasing weight ratio of BC to monomer (aniline and pyrrole), the curve area increased. Hence, the rectangle CV curve of BC/P(Ani-Py)1:1 composite modified electrode possessed higher integral area compared to that obtained from BC/P(Ani-Py)1:0.7 composite modified electrode (Fig. 4a). Obviously, increase of mixed monomer ratio in the preparation recipe increases the amount of electroactive P (Ani-Py) copolymer in composite and hence, increases the specific capacitance value, because the capacitance value is related directly to the integrated area of the CV curve (Liu et al., 2021). In other words, the higher the content of conducting copolymer formed on the surface of BC seed the higher is the possibility to form continuous conducting film. The more is the content of conductive copolymer the more dominant will be the occurrence of Faradaic redox reaction at the modified electrode–electrolyte interface.

Considering the performance of BC/P(Ani-Py)1:1 composite modified graphite electrode, the CV curve was further evaluated at various scan rates between 10 to 100 mV s^{-1}. The corresponding findings are displayed in Fig. 4b. Peak current response improves as scan rate is increased, and the shape of CV curves is nearly preserved. The BC/P (Ani-Py)1:1 composite electrode exhibits both performance and reversibility at high scan rates, indicating the material's efficacy as an electroactive material (Wang et al., 2017).

The same BC, P(Ani-Py), and BC/P(Ani-Py) modified graphite electrodes were utilized in subsequent CV and GCD experiments. During the measurement the electrolyte color was preserved i.e. dissolution/diffusion of electrode materials did not occur. These measurements were carried out at a fixed current density of 1.0 A g^{-1} in the potential window of −0.2 V to + 0.6 V (Fig. 5a). The type of electrode materials did not influence the symmetric nature of GCD curves and represent an almost linear relationship between the charge/discharge time and voltage. Such symmetrical shapes are attributable to the stabilized charge–discharge currents and suggest good capacitive behavior in reversible electrochemical transformations (Roldán et al., 2015; Han, & Cho, 2018). A negligible IR drop is observed at the start of the discharging phase, particularly for BC/P(Ani-Py)1:1 composite electrode, as illustrated in the inset of Fig. 5a, which normally originates from electrode internal resistance as well as solvent resistance. Compared to the BC and (Ani-Py), the IR drop obtained from respective composite modified electrode is lower and the discharge time increased indicating good capacitive properties. More importantly, the BC/P(Ani-Py)1:1 composite modified graphite electrode possessed the longest charge–discharge time and is thus attributable to the highest specific capacitance value. The specific capacitance values estimated from corresponding curves of BC, P(Ani-Py), BC/P(Ani-Py)1:0.7 and BC/P(Ani-Py)1:1 modified graphite electrodes at a fixed current density of 1.0 A g^{-1} are 100.0, 118.8, 188.50 and 274.3 F g^{-1} respectively. These results indicate that when the weight ratio of P(Ani-Py) to BC reached a suitable value, the electrochemical utilization ratio of BC would be strengthened and thus the electrochemical performance of the composite will be enhanced due to the synergistic effect.

The current density (0.5 to 3.0 A g^{-1}) dependent change in GCD potential for the best performed BC/P(Ani-Py)1:1 composite modified graphite electrode (Fig. 5b) was measured to check the rate capability. All curves show almost a triangular shape apart from a slight deviation from linear behavior. The charge–discharge time increases with a decrease in current density. In other word, the specific capacitance of BC/P(Ani-Py)1:1 composite material decreases with the increase of current density. This gradual decrease in specific capacitance with increasing current densities is related to the delayed charge diffusion, reduced faradaic redox reaction with the electroactive composite and inaccessible active surface area (Wang et al., 2017; Veerasubramani et al., 2016). Additionally, the limited electrochemical kinetics at a higher current density is also supposed to reduce the electrode efficiency

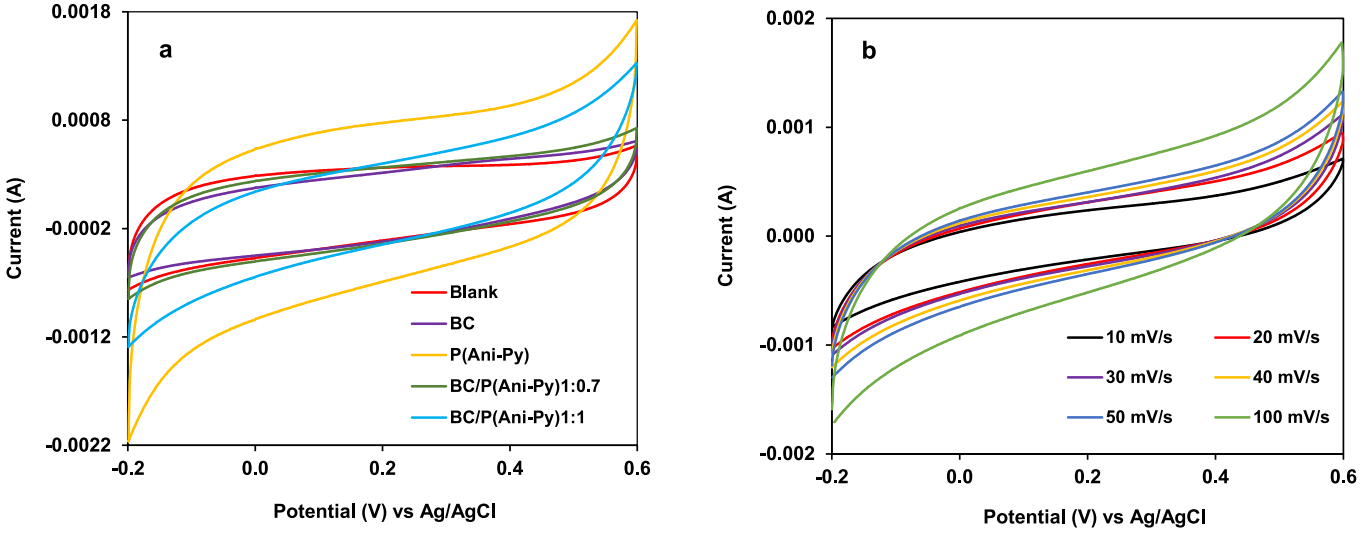

Fig. 4. (a) CV curves of blank electrode and graphite electrodes modified with BC seed particles, P(Ani-Py) particles, BC/P(Ani-Py)1:0.7 and BC/P(Ani-Py)1:1 composite particles at a scan rate of 50 mV/s; (b) CV curves of electrode modified with BC/P(Ani-Py)1:1 composite particles at variable scan rate.

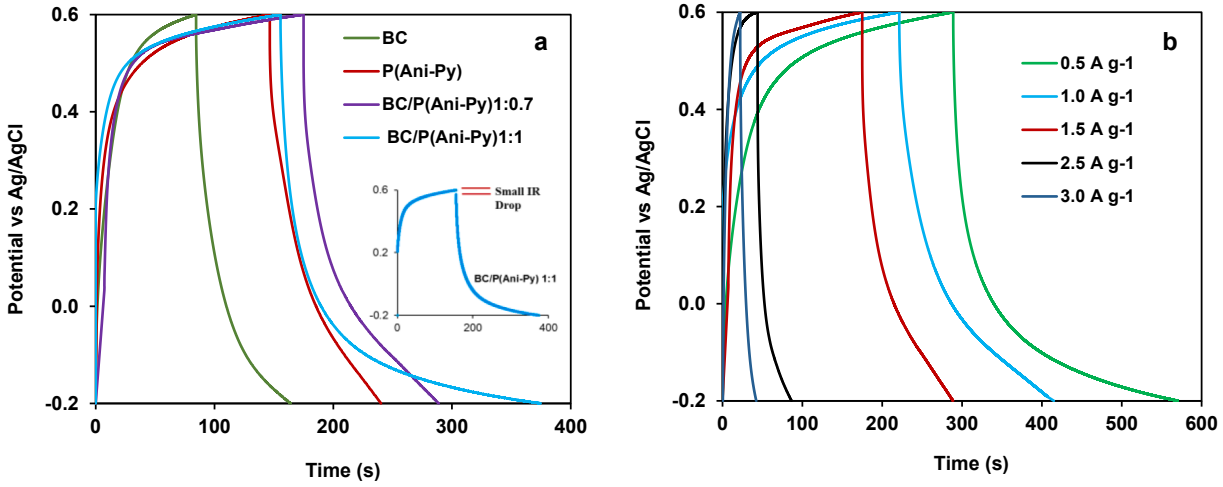

Fig. 5. (a) GCD curves of graphite electrodes modified with BC seed particles, P(Ani-Py) particles, BC/P(Ani-Py)1:0.7 and BC/P(Ani-Py)1:1 composite particles at fixed current density of 1.0 A/g; (b) GCD curves of graphite electrode modified with BC/P(Ani-Py)1:1 composite at different current densities.

(Gale et al., 2021). However, the effect of increased current density on the specific capacitance is less observed than expected, normally occurred for other conducting materials (Ali et al., 2022; Dhibar et al., 2015). This is one good side of BC as support materials for conducting P (Ani-Py) copolymer, because increasing amount of current density did not appreciably reduce the energy storage capacity of the composite modified graphite electrode. The –OH/ester/ether/carboxyl functionalities on BC seed provided active sides for binding with P(Ani-Py) copolymer particles. This binding between BC and conducting copolymer improved the network stability and compactness, which might have reduced the volume expansion–contraction at higher current density during charging-discharging operation. It is this resultant reduced degradation of conducting copolymer layer in the BC/P(Ani-Py) 1:1 composite particles perhaps produced less impact on capacitance value at higher current density. The BC/P(Ani-Py)1:1 composite particles exhibit higher electrical performance in terms of both CV and GCD measurements. This could potentially be attributed to the composite's higher electroactive P(Ani-Py) content than that in BC/P(Ani-Py)1:0.7. BC core in the composite provided physical strength as well as added synergistic effect to the composite electrode during faradic redox reaction.

The electrochemical impedance spectroscopy (EIS) of respective BC, P(Ani-Py), BC/P(Ani-Py)1:0.7, and BC/P(Ani-Py)1:1 modified graphite electrode was conducted for examination of the electrochemical diffusion process of each electrode material and the corresponding Nyquist plots are shown in Fig. 6. The plots of all EIS generally included two parts such as high frequency semicircle region and a low-frequency linear slope. The straight line in the low-frequency region gives information on the capacitance characteristics of modified electrode related to its diffusion resistance. The higher the slope of low-frequency straight line region, the better is the capacitance characteristic of electrode materials (Wang et al., 2020). Among all the Nyquist plots, the BC/P (Ani-Py)1:1 composite modified graphite electrode has given the largest slope, even more than the BC/P(Ani-Py)1:0.7 modified electrode (inset of Fig. 6). In either case the absence of semicircle region at higher frequencies indicates that modification of graphite electrode with our composites did not obstruct the flow of electrons from electrolyte to the interior of electrode. The electrical contact resistance or contact resistance (R_c), determines the resistance caused by incomplete contact through which the current is flowing, should be as low as possible to have reduced voltage drops and low circuit heating with increased current. The high-frequency intercept of the real axis (X-axis) gives the

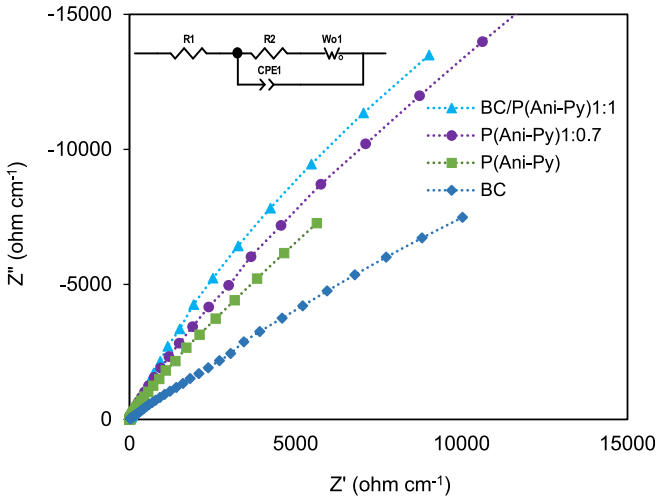

Fig. 6. The Nyquist plots of the EIS of BC seed particles, P(Ani-Py) particles, BC/P(Ani-Py)1:0.7 and BC/P(Ani-Py)1:1 composite particles in 1.0 M KCl solutions over the frequency range of 5×10^{-2} to 5×10^{-5} Hz measured at 50 mVs^{-1} scan rate. A sample equivalent circuit matched with the Nyquist plot of BC/P(Ani-Py)1:1 composite particles is shown in the inset of figure.

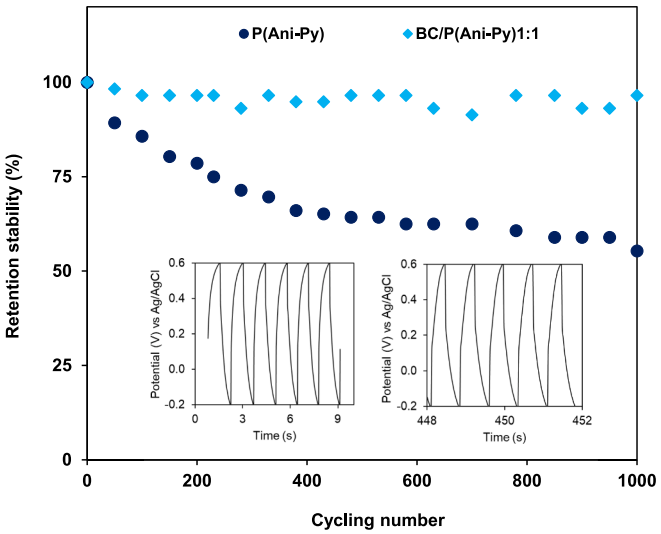

Fig. 7. Cycling stability of the reference P(An-Py) particles and BC/P(Ani-Py) 1:1 composite modified graphite electrode estimated from GCD curves in 1.0 M KCl solution. Inset shows the GCD curves for BC/P(Ani-Py)1:1 composite modified graphite electrode.

R_c (Girija & Sangaranarayanan, 2006). The R_c value of BC/P(Ani-Py)1:1 modified graphite electrode is noticeably low (4.0 Ω) compared to that of BC/P(Ani-Py)1:0.7 modified electrode (5.0 Ω), indicating fairly good contact at the interface. The Nyquist plot of the BC/P(Ani-Py)1:1 modified graphite electrode that matched with the equivalent circuit is shown in the inset of Fig. 6. In the equivalent circuit, R_1 represents the resistance of the outer layer known as the coating layer and R_2 represents the charge transfer resistance. The Warburg impedance W is attributed to the faradaic impedance. The constant phase element (CPE) and R_2 are in parallel connection and are referred to as the charge transfer limiting process. The values of parameters used for EIS data fitting of C/P(Ani-Py)1:1 modified graphite electrode are shown in Table S2.

The cycling stability, taken as an important parameter for determining the quality of energy storage materials, has been measured. The potential window of −0.2 V to + 0.6 V was kept similar to the preceding CV and GCD measurements. Considering the best electrochemical performance by BC/P(Ani-Py)1:1 modified graphite electrode, repeated GCD measurements were performed at a current density of 5.0 A g^{-1} and the retention of specific capacitance up to 1000 cycles is compared with that of reference P(An-Py) (Fig. 7). During the measurements change in electrolyte color as well as peeling of electrode materials from the electrode surface was not observed. A specific capacity retention of around 96.6 % after 1000 cycles showed pretty good cycle stability for the BC/P(Ani-Py)1:1 modified graphite electrode. This result mostly belongs to a mix of type I and type II cycle stability (Wu et al., 2021). This is because, the charge storage in BC/P(Ani-Py)1:1 modified graphite electrode is accompanied by both physical process of reversible adsorption–desorption of ions and reversible redox reaction at the electrode–electrolyte interface. In a previous experiment, Sahoo *et al.* observed a moderate capacitance retention of 66 % after 500 cycles for graphene/P(Ani-Py) nanocomposite particles (Sahoo et al., 2015), which is lower relative to our prepared modified graphite electrode. On the other, the retention of specific capacitance for the reference conductive copolymer modified electrode is only 55.4 % after 1000 cycles, which corresponds to type II cycle stability (Wu et al., 2021). This rapid decrease in specific capacity retention of P(Ani-Py) is generally accounted for the collapsed copolymer structure following severe volume expansion and contraction during charging and discharging process. In contrast, the rigid structure of BC/P(Ani-Py)1:1 has a negative influence on swelling and shrinkage of the copolymer volume during the repeated cycle. The improvement in stability following composite formation is associated with the formation of a rigid and stable structure due to hydrogen bonding interaction between BC and conducting copolymer. The fixation of BC based electroactive composite materials to graphite electrode is also apparently improved due to increased compatibility. This is to be mentioned that cycle stability is closely dependent on current density. The specific capacitance of BC/P(Ani-Py) 1:1 modified graphite electrode at the current density of 1.0 A g^{-1} is 274.3 F g^{-1}. But, at the current density of 5.0 A/g the initial specific capacitance value is obviously much low (6.25 F g^{-1}). This decrease in specific capacitance at higher current density is related to decrease in charge–discharge time and the real reason for such decrease is already outlined in the discussion of GCD curves (Fig. 5b).

In order to compare the performance with other popular energy storage devices, a relationship between the energy density and power

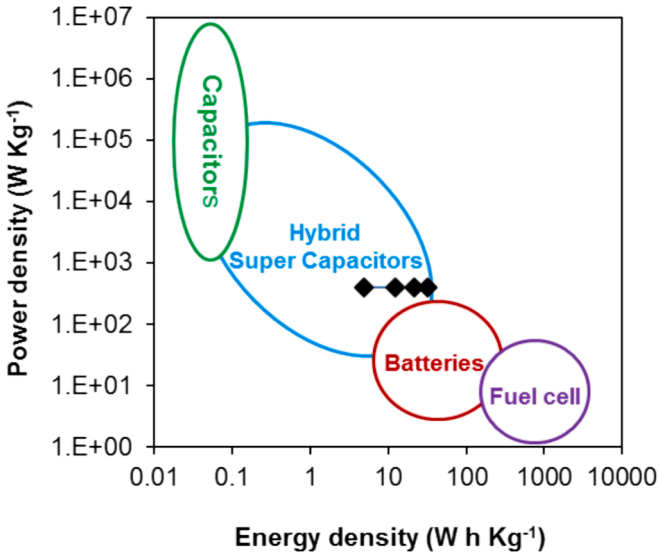

Fig. 8. Ragone plot of the BC/P(Ani-Py)1:1 composite modified graphite electrode in comparison with those of various electrochemical energy storage devices. Black spots represent density relationship corresponding to power density at different current densities of the BC/P(Ani-Py)1:1 composite electrode.

density of the BC/P(Ani-Py)1:1 composite electrode a Ragone plot (Fig. 8) is used (Ali et al., 2022; Libich et al., 2018). Our composite modified graphite electrode exhibits the maximum energy density of 31.5 W h Kg^{-1} at a power density of 400.0 W Kg^{-1}. It is evident that BC/P(Ani-Py)1:1 composite electrode possessed enough energy density with higher power density that make it conducive for application in energy storage devices. The energy density and power density values of the BC/P(Ani-Py)1:1 composite electrode are also compared with some recent carbon based materials (Table S3). It is evident that electrochemical performance of our composite modified electrode is comparable. Thus the designed BC supported conducting P(Ani-Py)1:1 copolymer can be attractive as a low-cost electrode material for supercapacitors of future generation. BC support can be evaluated for other polymer systems as well and there is also further scope to improve the electrochemical performance by using porous functional BC support for semi-conducting polymer and metals/metal ions.

4. Conclusion

In this investigation, for the first time, performance of conductive aniline-pyrrole copolymer functionalized BC modified graphite has been evaluated as low-cost electrode materials for application in next generation supercapacitor. Initially, the hydrothermal approach was employed to prepare micron-sized BC seed from 0.8 M sucrose aqueous solution. Finally, seeded chemical oxidative copolymerization of aniline and pyrrole was carried out in presence of BC at two different BC to mixed monomer weight ratios (1:0.7 and 1:1.0). The composites have been named as BC/P(Ani-Py)1:0.7 and BC/P(Ani-Py)1:1, respectively. BC seed is spherical and the average size is 2.56 μm. After composite formation the average sizes increased to 2.72 and 2.90 μm for weight ratios of 1:0.7 and 1:1.0 respectively. The smooth surface of BC seed particles turned rough and heterogeneous, which indicated formation of copolymer domains. The thermal stability of composites, independent of BC to mixed monomer ratio, laid between those of BC seed and reference copolymer particles. A comparative study of electrochemical performance from CV and GCD measurements showed better performance by BC/P(Ani-Py)1:1 modified graphite electrode. The capacitance values of graphite electrodes modified with each BC, P(Ani-Py), BC/P(Ani-Py) 1:0.7 and BC/P(Ani-Py)1:1, measured from GCD curves at a current density of 1.0 A g^{-1}, are 100.0, 118.8, 188.50 and 274.3F g^{-1}, respectively. It is obvious that BC support for copolymer improved the performance of the electrode via synergistic effect and improved stability. The higher weight ratio of BC to mixed monomer had also positive effect on the capacitance value. Importantly, the increase of current density produced small effect on the decreasing trend of specific capacitance for composite modified graphite electrode. The best performed BC/P(Ani-Py)1:1 modified graphite electrode produced a maximum energy density of 21.62 W h Kg^{-1} at a power density of 400.0 W Kg^{-1}. The capacitance retention of the BC/P(Ani-Py)1:1 composite graphite electrode is 96.6 % after 1000 charge/discharge cycles, indicating a very good stability. In summary, BC support materials can be useful for decorating with electroactive polymer in designing electrode materials for potential applications in supercapacitors as a next generation low cost energy storage devices. At the end, there is also ample scope to further enhance the electrochemical performance of BC/P(Ani-Py) composite modified electrode by using functional porous BC support materials as this will enhance electrode–electrolyte contact area and boost the binding between BC support and conducting polymer through enhanced compatibility as well as increased interfacial area.

CRediT authorship contribution statement

Md. Mahabur Rahman: Writing – original draft, Validation, Methodology, Investigation, Formal analysis, Data curation. **Abdulla Al Mamun:** Validation, Methodology, Investigation, Formal analysis, Data curation. **Hideto Minami:** Investigation, Data curation. **Md. Mahbubor Rahman:** Funding acquisition, Conceptualization. **S. Manjura Hoque:** Investigation, Data curation. **Hasan Ahmad:** Writing – review & editing, Supervision, Resources, Project administration, Data curation, Conceptualization.

Declaration of competing interest

The authors declare that they have no known competing financial interests or personal relationships that could have appeared to influence the work reported in this paper.

Acknowledgment

The author (HA) acknowledges research grant under special allocation (FY 2021-2022) from Rajshahi University.

Appendix A. Supplementary data

Supplementary data to this article can be found online at https://doi.org/10.1016/j.arabjc.2024.105938.

References

Aboughaly, M., Babaei-Ghazvini, A., Dhar, P., Patel, R., Acharya, B., 2023. Enhancing the potential of polymer composites using biochar as a filler: a review. Polymers 15 (19), 3981. https://doi.org/10.3390/polym15193981.

Ahmad, H., Rahman, M.M., Ali, M.A., Minami, H., Tauer, K., Gafur, M.A., Rahman, M.M., 2016. A simple route to synthesize conductive stimuli-responsive polypyrrole nanocomposite hydrogel particles with strong magnetic properties and their performance for removal of hexavalent chromium ions from aqueous solution. J. Magnet. Magnet. Mater. 412, 15–22. https://doi.org/10.1016/j.jmmm.2016.03.068.

Ali, M.S., Rahman, M.M., Hossain, M.K., Minami, H., Rahman, M.M., Hoque, S.M., Alam, M.A., Ahmad, H., 2022. Impact of mesoporous SiO_2 support for Ni/polypyrrole nanocomposite particles on their capacitive performance. New J. Chem. 46 (45), 21798–21811. https://doi.org/10.1039/D2NJ04320C.

Antony, M.J., Jayakannan, M., 2011. Role of anionic micellar template on the morphology, solid-state ordering, and unusual conductivity trend ordering, and unusual conductivity trend in poly(aniline-*co*-pyrrole) nanomaterials. J. Phys. Chem. B 115 (20), 6427–6436. https://doi.org/10.1021/jp2015726.

Chaudhary, V., Kaur, A., 2015. Enhanced and selective ammonia sensing behaviour of poly(aniline co-pyrrole) nanospheres chemically oxidative polymerized at low temperature. J. Ind. Eng. Chem. 26, 143–148. https://doi.org/10.1016/j.jiec.2014.11.026.

Debnath, M.K., Rahman, M.A., Minami, H., Rahman, M.M., Alam, M.A., Sharafat, M.K., Hossain, M.K., Ahmad, H., 2019. Single step modification of micrometer-sized polystyrene particles by electromagnetic polyaniline and sorption of chromium(VI) metal ions from water. J. Appl. Polym. Sci. 136 (19), 47524. https://doi.org/10.1002/app.47524.

Dhibar, S., Bhattacharya, P., Hatui, G., Das, C.K., 2015. Transition metal doped poly (aniline-*co*-pyrrole)/multi-walled carbon nanotubes nanocomposite for high performance supercapacitor electrode materials. J. Alloys Compds. 625, 64–75. https://doi.org/10.1016/j.jallcom.2014.11.108.

Dong, J., Yang, Q., Zhao, Q., Hou, Z., Zhou, Y., Zhang, R., 2020. Poly(aniline-co-pyrrole)-coated Ni-doped manganese dioxide as electrode materials for supercapacitors. Funct. Mater. Lett. 13 (02), 2051007 https://doi.org/10.1142/S1793604720510078.

Gale, M., Nguyen, T., Moreno, M., Gilliard-AbdulAziz, K.L., 2021. Physiochemical properties of biochar and activated carbon from biomass residue: influence of process conditions to adsorbent properties. ACS Omega 6 (15), 10224–10233. https://doi.org/10.1021/acsomega.1c00530.

Gao, Y., Zhang, Y., Li, A., Zhang, L., 2018. Facile synthesis of high-surface area mesoporous biochar for energy storage via *in-situ* template strategy. Mater. Lett. 230, 183–186. https://doi.org/10.1016/j.matlet.2018.07.106.

Girija, T.C., Sangaranarayanan, M.V., 2006. Analysis of polyaniline-based nickel electrodes for electrochemical supercapacitors. J. Power Sources 156 (2), 705–711. https://doi.org/10.1016/j.jpowsour.2005.05.051.

Golczak, S., Kanciurzewska, A., Fahlman, M., Langer, K., Langer, J.J., 2008. Comparative XPS surface study of polyaniline thin films. Solid State Ion. 179, 2234–2239.

Govindaraju, K.M., Prakash, V.C.A., 2015. Synthesis of zinc modified poly(aniline-co-pyrrole) coating and its anti-corrosive performance on low nickel stainless steel. Colloids Surfaces a: Physicochem. Eng. Asp. 465, 11–19. https://doi.org/10.1016/j.colsurfa.2014.10.011.

Hajiabdolah, N., Parsa, A., Anaraki-Ardakani, H., Jalali-Jahromi, H., 2020. Iron(III) reduction as a measure of "antioxidant power" using homo and copolymer of pyrrole and aniline electrosynthesized. Rev. Roum. Chim. 65 (3), 247–254. https://doi.org/10.33224/rrch.2020.65.3.04.

Hammad, A.S., Noby, H., Elkady, M.F., El-Shazly, A.H., 2018. In-situ polymerization of polyaniline/polypyrrole copolymer using different techniques. IOP Conf. Series:

Mater. Sci. Eng. 290 (1), 012001 https://doi.org/10.1088/1757-899X/290/1/012001.
Han, H., Cho, S., 2018. Ex situ fabrication of polypyrrole-coated core-shell nanoparticles for high-performance coin cell supercapacitor. Nanomaterials 8 (9), 726. https://doi.org/10.3390/nano8090726.
Hara, M., Yoshida, T., Takagaki, A., Takata, T., Kondo, J.N., Hayashi, S., Domen, K., 2004. A carbon material as a strong protonic acid. Angew. Chem. Int. Ed. 43 (22), 2955–2958. https://doi.org/10.1002/anie.200453947.
He, M., Xu, Z., Hou, D., Gao, B., Cao, X., Ok, Y.S., Rinklebe, J., Bolan, N.S., Tsang, D.C., 2022. Waste-derived biochar for water pollution control and sustainable development. Nat. Rev. Earth Environ. 3 (7), 444–460. https://doi.org/10.1038/s43017-022-00306-8.
Hou, F., Gorthy, R., Mardon, I., Tang, D., Goode, C., 2022. Low voltage environmentally friendly plasma electrolytic oxidation process for titanium alloy. Sci. Reports 12, 6037. https://doi.org/10.1038/s41598-022-09693-w.
Idrees, M., Jeelani, S., Rangari, V., 2018. Three-dimensional-printed sustainable biochar-recycled PET composites. ACS Sustainable Chem. Eng. 6 (11), 13940–13948. https://doi.org/10.1021/acssuschemeng.8b02283.
Khan, M.M.R., Islam, M., Amin, M.K., Paul, S.K., Rahman, S., Talukder, M.M., Rahman, M.M., 2022. Simplistic fabrication of aniline and pyrrole-based poly(Ani-co-Py) for efficient photocatalytic performance and supercapacitors. Int. J. Hydrogen Energy 47 (89), 37860–37869. https://doi.org/10.1016/j.ijhydene.2022.08.296.
Kim, M., Goerzen, D., Jena, P.V., Zeng, E., Pasquali, M., Meidl, R.A., Heller, D.A., 2024. Human and environmental safety of carbon nanotubes across their life cycle. Nat. Rev. Mater. 9 (1), 63–81. https://doi.org/10.1038/s41578-023-00611-8.
Kim, J., Lee, J., You, J., Park, M.S., Al Hossain, M.S., Yamauchi, Y., Kim, J.H., 2016. Conductive polymers for next-generation energy storage systems: recent progress and new functions. Mater. Horiz. 3 (6), 517–535. https://doi.org/10.1039/C6MH00165C.
Kim, S., Oh, J.S., Hwang, T., Seo, H.W., Jeong, D.C., Lee, J.H., Wen, L., Song, C., Han, J. G., Nam, J.D., 2019. Synchronous polymerization of 3.4-ethylenedioxythiophene and pyrrole by plasma enhanced chemical vapor deposition (PECVD) for conductive thin film with tunable energy bandgap. Macromol. Res. 27 (3), 243–249. https://doi.org/10.1007/s13233-019-7045-0.
Labbé, N., Harper, D., Rials, T., Elder, T., 2006. Chemical structure of wood charcoal by infrared spectroscopy and multivariate analysis. J. Agric. Food Chem. 54 (10), 3492–3497. https://doi.org/10.1021/jf053062n.
Li, B., Liu, D., Lin, D., Xie, X., Wang, S., Xu, H., Wang, J., Huang, Y., Zhang, S., Hu, X., 2020. Changes in biochar functional groups and its reactivity after volatile-char interactions during biomass pyrolysis. Energy Fuels 34 (11), 14291–14299. https://doi.org/10.1021/acs.energyfuels.0c03243.
Libich, J., Máca, J., Vondrák, J., Čech, O., Sedlaříková, M., 2018. Supercapacitors: properties and applications. J. Energy Storage 17, 224–227. https://doi.org/10.1016/j.est.2018.03.012.
Lim, V.W.L., Kang, E.T., Neoh, K.G., Ma, Z.H., Tan, K.L., 2001. Determination of pyrrole-aniline copolymer compositions by X-ray photoelectron spectroscopy. Appl. Surf. Sci. 181 (3–4), 317–326. https://doi.org/10.1016/S0169-4332(01)00428-7.
Lin, Y., Li, F., Li, X., Zhao, H., Liu, G., 2023. Multifunctional template prepares N-, O- and S- codoped mesoporous 3D hollow nanocage biochar with a multilayer wall structure for aqueous high-performance supercapacitors. ACS Appl. Energy Mater. 6 (4), 2265–2275. https://doi.org/10.1021/acsaem.2c03427.
Liu, B., Sun, H., Peng, T., Zhi, X., 2021. 3-D Core-shell poly(aniline-co-pyrrole)/reduced graphene oxide composite for supercapacitor performance. Diamond Related Mater. 118 (2021), 108498 https://doi.org/10.1016/j.diamond.2021.108498.
Lopes, R.P., Astruc, D., 2021. Biochar as a support for nanocatalysts and other reagents: recent advances and applications. Coordination Chem. Rev. 426, 213585 https://doi.org/10.1016/j.ccr.2020.213585.
Lu, W., Yin, S., Wu, X., Luo, Q., Wang, E., Cui, L., Guo, C.Y., 2021. Aniline-pyrrole copolymers formed on single-walled carbon nanotubes with enhanced thermoelectric performance. J. Mater. Chem. C 9 (8), 2898–2903. https://doi.org/10.1039/D0TC05757F.
Lv, L., Huang, S., Zhou, H., 2024. Effect of introducing chemically activated biochar as support materials on thermal properties of different organic phase change materials. Solar Energy Mater. Solar Cells 264, 112617. https://doi.org/10.1016/j.solmat.2023.112617.
Lv, D., Shen, W., Chen, W., Wang, Y., Tan, R., Zhao, M., Song, W., 2023. Emerging poly (aniline-co-pyrrole) nanocomposites by in-situ polymerized for high-performance flexible ammonia sensor. Sens. Act. A: Phys. 349, 114078 https://doi.org/10.1016/j.sna.2022.114078.
Lyu, H., Zhang, Q., Shen, B., 2020. Application of biochar and its composites in catalysis. Chemosphere 240, 124842. https://doi.org/10.1016/j.chemosphere.2019.124842.
Ma, A.N., Wang, B., Zheng, Y., Yang, H., Ma, Q.F., Deng, S.H., 2023. Electrochemical synthesis and energy storage study of aniline-pyrrole conductive copolymer electrode. J. Energy Storage 72, 108242. https://doi.org/10.1016/j.est.2023.108242.
Mehmandoust, M., Li, G., Erk, N., 2022. Biomass-derived carbon materials as an emerging platform for advanced electrochemical sensors: recent advances and future perspectives. Ind. Eng. Chem. Res. 62, 4628–4635. https://doi.org/10.1021/acs.iecr.2c03058.
Moyseowicz, A., González, Z., Menéndez, R., Gryglewicz, G., 2018. Three-dimensional poly(aniline-*co*-pyrrole)/thermally reduced graphene oxide composite as a binder-free electrode for high performance supercapacitors. Comp. Part B: Eng. 145, 232–239. https://doi.org/10.1016/j.compositesb.2018.03.018.
Moyseowicz, A., Minta, D., Gryglewicz, G., 2023. Conductive polymer/graphene-based composites for next generation energy storage and sensing applications. ChemElectroChem 10 (9), e20220115.
Muthulakshmi, B., Kalpana, D., Pitchumani, S., Renganathan, N.G., 2006. Electrochemical deposition of polypyrrole for symmetric supercapacitors. J. Power Sources 158 (2), 1533–1537. https://doi.org/10.1016/j.jpowsour.2005.10.013.
Nguyen, T.B., Sherpa, K., Bui, X.T., Nguyen, V.T., Chen, C.W., Dong, C.D., 2023. Biochar for soil remediation: a comprehensive review of current research on pollutant removal. Environ. Pollut. 337, 122571 https://doi.org/10.1016/j.envpol.2023.122571.
Oliveira, R.D., Santos, C.S., Hryniewicz, B.M., Marchesi, L.F., Pessoa, C.A., 2024. Evaluation of supercapacitive properties of a PPY/PANI bilayer electrodeposited onto carbon-graphite electrodes obtained from spent batteries. Processes 12 (1), 31. https://doi.org/10.3390/pr12010031.
Papadopoulou, K., Klonos, P.A., Kyritsis, A., Mašek, O., Wurzer, C., Tsachouridis, K., Anastasiou, A.D., Bikiaris, D.N., 2023. Synthesis and study of fully biodegradable composites based on poly(butylene succinate) and biochar. Polymers 15 (4), 1049. https://doi.org/10.3390/polym15041049.
Park, W., Kim, H., Park, H., Choi, S., Hong, S.J., Bahk, Y.M., 2021. Biochar as a low-cost, eco-friendly, and electrically conductive material for terahertz applications. Sci. Reports 11 (1), 18498. https://doi.org/10.1038/s41598-021-98009-5.
Rahman, S., Khan, M.M.R., Deb, B., Dana, S.I., Ahmed, M.K., 2023. Effective and simple fabrication of pyrrole and thiophene-based poly(Py-co-Th)/ZnO composites for high photocatalytic performance. South Afr. J. Chem. Eng. 43, 303–311. https://doi.org/10.1016/j.sajce.2022.11.010.
Rashid, M., Islam, M.M., Minami, H., Aftabuzzaman, M., Rahman, M.A., Hossain, M.M., Hoque, S.M., Alam, M.A., Ahmad, H., 2020. Nickel decorated melamine-formaldehyde resin/polyaniline composites for high specific capacitance. Mater. Chem. Phys. 249, 122957 https://doi.org/10.1016/j.matchemphys.2020.122957.
Roldán, S., Barreda, D., Granda, M., Menéndez, R., Santamaría, R., Blanco, C., 2015. An approach to classification and capacitance expressions in electrochemical capacitors technology. Phys. Chem. Chem. Phys. 17 (2), 1084–1092. https://doi.org/10.1039/C4CP05124F.
Saharan, P., Singh, M., Kumar, C., Sundriyal, S., Dhakate, S.R., 2023. Highly nanoporous activated carbon derived from poly(aniline-*co*-pyrrole) for electrochemical capacitors. ACS Appl. Nano Mater. 6 (23), 21909–21921. https://doi.org/10.1021/acsanm.3c04128.
Sahoo, S., Bhattacharya, P., Dhibar, S., Hatui, G., Das, T., Das, C.K., 2015. Graphene/Poly (aniline-co-pyrrole) nanocomposite: potential candidate for supercapacitor and microwave absorbing applications. J. Nanosci. Nanotechnol. 15 (9), 6931–6941. https://doi.org/10.1166/jnn.2015.10540.
Sankar, S., Ramesan, M.T., 2022. Synthesis, characterization, conductivity, and gas-sensing performance of copolymer nanocomposites based on copper alumina and poly(aniline-co-pyrrole). Polym. Eng. Sci. 62 (8), 2402–2410. https://doi.org/10.1002/pen.26014.
Sevilla, M., Fuertes, A.B., 2009. Chemical and structural properties of carbonaceous products obtained by hydrothermal carbonization of saccharides. Chem. Eur. J. 15 (16), 4195–4203.
Sun, L., Chen, D., Wan, S., Yu, Z., 2018. Adsorption studies of dimetridazole and metronidazole onto biochar derived from sugarcane bagasse: kinetic, equilibrium, and mechanisms. J. Polym. Environ. 26, 765–777. https://doi.org/10.1007/s10924-017-0986-5.
Sun, L., Yin, Z., Zhang, J., Ren, X., Zhang, M., Song, W., Xu, Z., Qi, C., 2022. Gold nanoparticles supported on poly(aniline-co-pyrrole) as the efficient catalysts for the reduction of 4-nitrophenol. Mol. Catal. 525, 112362 https://doi.org/10.1016/j.mcat.2022.112362.
Tan, G., Yu, H.Q., 2024. Rethinking biochar: black gold or not? Nature Rev. Mater. 9 (1), 4–5. https://doi.org/10.1038/s41578-023-00634-1.
Thi, Q.V., Lim, S., Jang, E., Kim, J., Van Khoi, N., Tung, N.T., Sohn, D., 2020. Silica particles wrapped with poly(aniline-co-pyrrole) and reduced graphene oxide for advanced microwave absorption. Mater. Chem. Phys. 244, 122691 https://doi.org/10.1016/j.matchemphys.2020.122691.
Veerasubramani, G.K., Krishnamoorthy, K., Radhakrishnan, S., Kim, N.J., Kim, S.J., 2016. In-situ chemical oxidative polymerization of aniline monomer in the presence of cobalt molybdate for supercapacitor applications. J. Ind. Eng. Chem. 36, 163–168. https://doi.org/10.1016/j.jiec.2016.01.031.
Visser, E.D., Seroka, N.S., Khotseng, L., 2023. Catalytic properties of biochar as support material potential for direct methanol fuel cell: a review. ACS Omega 8 (44), 40972–40981. https://doi.org/10.1021/acsomega.3c02283.
Wang, S., Liu, F., Gao, C., Wan, T., Wang, L., Wang, L., Wang, L., 2019. Enhancement of the thermoelectric property of nanostructured polyaniline/carbon nanotube composites by introducing pyrrole unit onto polyaniline backbone via a sustainable method. Chem. Eng. J. 370, 322–329. https://doi.org/10.1016/j.cej.2019.03.155.
Wang, Y., Ma, W.B., Guo, L., Song, X.Z., Tao, X.Y., Guo, L.T., Fan, H.L., Liu, Z.S., Zhu, Y. B., Wei, X.Y., 2020b. Phytic acid-doped poly(aniline-co-pyrrole) copolymers for supercapacitor electrodes applications. J. Mater. Sci.: Mater Electronics 31, 6263–6273. https://doi.org/10.1007/s10854-020-03181-5.
Wang, S., Mao, M., Cao, Y., Luo, H., Wang, H., Guo, D., 2020a. Novel cuboid-like cobalt nickel phosphate/manganese dioxide/multi-walled carbon nanotubes composites as binder-free electrodes for high-performance supercapacitors. Inorg. Chem. Commun. 114, 107822 https://doi.org/10.1016/j.inoche.2020.107822.
Wang, J., Zhang, X., Zhang, Y., Abas, A., Zhao, X., Yang, Z., Su, Q., Lan, W., Xie, E., 2017. Lightweight, interconnected VO_2 nanoflowers hydrothermally grown on 3D graphene networks for wide-voltage-window supercapacitors. RSC Adv. 7 (56), 35558–35564. https://doi.org/10.1039/C7RA04376G.
Wu, Q., He, T., Zhang, Y., Zhang, J., Wang, Z., Liu, Y., Zhao, L., Wu, Y., Ran, F., 2021. Cyclic stability of supercapacitors: materials, energy storage mechanism, test methods, and device. J. Mater. Chem. A 9 (43), 24094–24147. https://doi.org/10.1039/D1TA06815F.

Xue, B., Xu, J., Feng, Y., Ma, M., Xiao, R., Wang, X., 2023. Morphology engineering of biomass-derived porous carbon from 3D to 2D towards boosting capacitive charge storage capability. J. Colloid Interface Sci. 642, 736–746. https://doi.org/10.1016/j.jcis.2023.03.200.

Yan, J., Fang, Y., Wang, S., Wu, S., Wang, L., Zhang, Y., Luo, H., Cao, Y., Gao, H., Wang, L.-Z., Liu, F.-J., 2020. Nitrogen-doped oxygen-rich activated carbon derived from longan shell for supercapacitors. Int. J. Electrochem. Sci. 15, 1982–1995. https://doi.org/10.20964/2020.03.18.

Yasim-Anuar, T.A.T., Yee-Foong, L.N., Lawal, A.A., Farid, M.A.A., Yusuf, M.Z.M., Hassan, M.A., Ariffin, H., 2022. Emerging application of biochar as a renewable and superior filler as polymer composites. RSC Adv. 12 (22), 13938–13949. https://doi.org/10.1039/D2RA01897G.

Zhang, Y., Xue, S., Yan, X., Gao, H.-L., Gao, K., 2023. Preparation and electrochemical properties of cobalt aluminum layered double hydroxide/carbon-based integrated composite electrode materials for supercapacitors. Electrochim. Acta 442, 141822. https://doi.org/10.1016/j.electacta.2023.141822.

Zhang, Y., Zhou, C., Yan, X., Cao, Y., Gao, H., Luo, H., Gao, K., Xue, S., Jing, X., 2023a. Recent advances and perspectives on graphene-based gels for superior flexible all-solid-state supercapacitors. J. Power Sources 565, 232916. https://doi.org/10.1016/j.jpowsour.2023.232916.

Zhang, Y., Jing, X., Yan, X., Gao, H., Gao, K., Cao, Y., Hu, S., Zhang, Y., 2024b. Rational design of NiMn-based electrode materials for high-performance supercapacitors. Coordination Chem. Rev. 499, 215494 https://doi.org/10.1016/j.ccr.2023.215494.

Zhou, C., Han, J., Song, G., Guo, R., 2008. Fabrication of poly(aniline-*co*-pyrrole) hollow nanospheres with triton x–100 micelles as templates. J. Polym. Sci.: Part A: Polym. Chem. 46 (11), 3563–3572. https://doi.org/10.1002/pola.22695.